Dynamical mean-field theory for flat-band ferromagnetism

Hong-Son Nguyen
Department of Occupational Safety and Health, Trade Union University, 169 Tay Son, Hanoi, Vietnam

Minh-Tien Tran
Institute of Research and Development, Duy Tan University, K7/25 Quang Trung, Danang, Vietnam
and Institute of Physics, Vietnam Academy of Science and Technology, 10 Dao Tan, Hanoi, Vietnam
(Received 14 March 2016; revised manuscript received 23 August 2016; published 6 September 2016)

The magnetically ordered phase in the Hubbard model on the infinite-dimensional hyper-perovskite lattice is investigated within dynamical mean-field theory. It turns out for the infinite-dimensional hyper-perovskite lattice the self-consistent equations of dynamical mean-field theory are exactly solved, and this makes the Hubbard model exactly solvable. We find electron spins are aligned in the ferromagnetic or ferrimagnetic configuration at zero temperature and half filling of the edge-centered sites of the hyper-perovskite lattice. A ferromagnetic-ferrimagnetic phase transition driven by the energy level splitting is found and it occurs through a phase separation. The origin of ferromagnetism and ferrimagnetism arises from the band flatness and the virtual hybridization between macroscopically degenerate flat bands and dispersive ones. Based on the exact solution in the infinite-dimensional limit, a modified exact diagonalization as the impurity solver for dynamical mean-field theory on finite-dimensional perovskite lattices is also proposed and examined.

DOI: 10.1103/PhysRevB.94.125106

I. INTRODUCTION

Recently, flat (dispersionless) band systems have received a great deal of attention due to the emergence of electron correlations in macroscopic degeneracy. The emergence can lead to rich strongly correlated phenomena [1]. The fractional quantum Hall effect without external magnetic field and flat-band ferromagnetism are its preeminent examples [2–7]. In the flat bands the electron wave functions are well localized in real space, and this localization quenches the kinetic energy, leaving the Coulomb interaction between electrons as the dominant force. As a result electrons tend to be spin polarized to minimize the interaction energy without any cost in the kinetic energy. This yields the flat-band ferromagnetism [8,9]. Actually, it is a limit realization of the Stoner criterion of ferromagnetism, where the density of states becomes infinite [10]. Flat-band ferromagnetism can be considered as the complement to Nagaoka ferromagnetism, where the Stoner criterion is realized by infinite Coulomb interactions [11]. Several experimental realizations of flat-band ferromagnetism in quantum wires [12], quantum dot arrays [13], and ultracold fermion systems [14,15] have already been proposed.

Theoretically, a nontrivial flat band exists when the electron hopping remains finite, but the net hopping vanishes. This destructive interference can be realized by cell construction [8,9], line graphs [16–18], or orbital selection [19,20]. One of the simplest flat-band models is the tight-binding model on the so-called Lieb lattice or the edge-centered square lattice. It belongs to the model family of cell construction [1,8]. The Lieb lattice has attracted a lot of research attention since it is the essential structure of layered cuprates of high-temperature superconductors, and recently it was also experimentally realized [21]. The edge-centered cubic lattice is also found in the perovskite structure [22]. In the cubic perovskite compounds ABX_3, their essential structure elements, the corner-sharing octahedra BX_6, form the edge-centered cubic lattice (see Fig. 1). Sometimes, the three-dimensional edge-centered cubic lattice is also referred to as the perovskite lattice [23]. Recently, ferromagnetism was found in a number of transition-metal-oxide-based perovskites [24–29]. Studying correlation effects in the perovskite lattice would reveal the nature of magnetic ordering. We will refer to the edge-centered hypercubic lattice as the hyper-perovskite lattice.

Electron correlations in the hyper-perovskite lattices can lead the system to a wide variety of physics including magnetism, superfluidity, and topological phases [8,15,23,30]. The simplest model for correlated electrons is the Hubbard model. Originally, the Hubbard model was introduced to explore the origin of ferromagnetism [31–33]. However, for most common lattices, the stability of ferromagnetism in the Hubbard model is very limited [11,34]. It turns out that the Hubbard model is a generic model rather for antiferromagnetism than for ferromagnetism. However, on the flat-band lattices the ferromagnetic stability may occur in a wide parameter space, since the Stoner criterion for ferromagnetism is satisfied [8]. In addition, on the hyper-perovskite lattices ferromagnetism or ferrimagnetism is more preferable than antiferromagnetism due to unequal numbers of sublattice sites [35].

In general, the stability of ferromagnetism in the Hubbard model requires nonperturbative approaches [34]. Dynamical mean-field theory (DMFT) is a powerful nonperturbative tool, and it is widely and successfully used to investigate correlation effects [36,37]. DMFT is exact in the infinite-dimensional limit. The ferromagnetic stability in the Hubbard model on the two-dimensional hyper-perovskite lattice was already investigated by using the DMFT [15]. However, due to the flat-band feature, the dynamical mean field must properly retain the small energy scale. So far, only the numerical renormalization group (NRG) is capable of capturing the low-energy properties [15]. The standard exact diagonalization (ED) [37,38] may fail to reproduce the dynamical mean field from the finite set of bath orbits. However, by considering the DMFT for the perovskite lattice in the infinite-dimensional limit, we find that the self-consistent equations of the DMFT

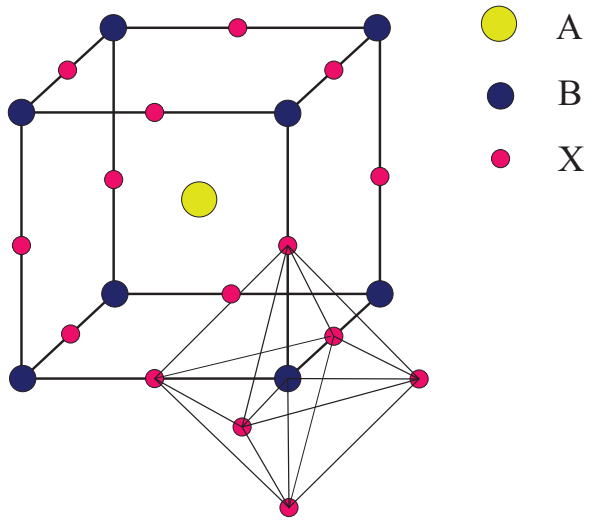

FIG. 1. The ideal structure of perovskite compounds ABX_3. The corner-sharing octahedra BX_6 form an edge-centered cubic lattice.

are exactly solvable. This allows us to explicitly construct the effective impurity model, which exactly treats the low-energy scale in the infinite-dimensional limit. The exact solution of the Hubbard model on the infinite-dimensional hyper-perovskite lattice gives a precise insight of the magnetically ordered ground state and the origin of magnetism in the flat-band systems. In addition to the one-dimensional lattice, the infinite-dimensional hyper-perovskite lattice is the other unique case, where the Hubbard model is exactly solved. Moreover, based on the tractable analysis of the DMFT at the infinite-dimensional limit, we also propose a modified ED scheme for the DMFT on finite-dimensional perovskite lattices. In contrast to the standard ED [37,38], the modified ED well recovers the NRG results. It could be used as an alternative impurity solver to the NRG for the DMFT on the finite-dimensional perovskite lattices. The modified ED can be implemented into the density functional theory (DFT) plus DMFT for the electronic structure calculations [39,40].

The present paper is organized as follows. In Sec. II we present the DMFT for the Hubbard model on the hyper-perovskite lattice. In this section we also present the exact solution of the DMFT at the infinite-dimensional limit and its application for finite-dimensional perovskite lattices. Finally, Sec. III is the conclusion.

II. THE HUBBARD MODEL ON THE HYPER-PEROVSKITE LATTICE AND ITS DYNAMICAL MEAN-FIELD THEORY SOLUTION

We consider the Hubbard model on the d-dimensional hyper-perovskite lattice

$$H = -t \sum_{\langle i,j\rangle,\sigma} c^\dagger_{i\sigma} c_{j\sigma} + U \sum_i c^\dagger_{i\uparrow} c_{i\uparrow} c^\dagger_{i\downarrow} c_{i\downarrow}, \tag{1}$$

where $c^\dagger_{i\sigma}$ ($c_{i\sigma}$) is the electron creation (annihilation) operator with spin σ at site i. t is the hopping parameter and we take into account only the hopping between nearest-neighbor sites. U is the local Coulomb interaction. The d-dimensional hyper-perovskite lattice consists of a d-dimensional hypercubic lattice and additional sites located in the middle of every edge of the hypercube. In the two-dimensional space the hyper-perovskite lattice is also called the Lieb lattice [1]. The Lieb lattice is essentially the structure of layered cuprates, and recently it was realized by an array of optical waveguides [21]. The three-dimensional perovskite lattice can be found in perovskite compounds [22]. The hyper-perovskite lattice is bipartite. We denote its sublattices by C and A, where C is the hypercube, and A is the sublattice of the edge middle sites. The unit cells of the hyper-perovskite lattice are the unit cells of the hypercubic lattice and they consist of one site of the hypercube C and its d nearest-neighbor sites of the A sublattice. We also denote the number of sites of the hypercube C by N_C. The Hamiltonian in Eq. (1) can be rewritten as

$$\begin{aligned} H = &-t \sum_{I,l,\sigma} c^\dagger_{I\sigma} a_{Il\sigma} + \text{H.c.} + \sum_{I\sigma} (\varepsilon_c - \mu_\sigma) c^\dagger_{I\sigma} c_{I\sigma} \\ &- \sum_{Il\sigma} \mu_\sigma a^\dagger_{Il\sigma} a_{Il\sigma} + U \sum_I n^c_{I\uparrow} n^c_{I\downarrow} + U \sum_{Il} n^a_{Il\uparrow} n^a_{Il\downarrow}, \end{aligned} \tag{2}$$

where c and a denote the electron operator for the sublattices C and A, respectively. The site index I runs over the lattice sites of the hypercube C. $l = 1,2,\ldots,d$ are the site indices of the nearest-neighbor sites of the sublattice A around the site I of the hypercube C. $n^a_{Il\sigma} = a^\dagger_{Il\sigma} a_{Il\sigma}$, $n^c_{I\sigma} = c^\dagger_{I\sigma} c_{I\sigma}$ are the number operators of electrons in the A and C sublattices. $\mu_\sigma = \mu + \sigma h$. Here we explicitly introduce the chemical potential μ and an external magnetic field h. ε_c is the energy level for electrons in the hypercube C. We also set the lattice parameter of the hypercube as the length unit.

A. Free fermions in the infinite-dimensional hyper-perovskite lattice

First, we consider the noninteracting case ($U = 0$). We introduce the vector

$$\Psi_{I\sigma} = \begin{pmatrix} c_{I\sigma} \\ a_{I1\sigma} \\ \vdots \\ a_{Id\sigma} \end{pmatrix} \tag{3}$$

and its Fourier transform in momentum space $\Psi_{\mathbf{k}\sigma}$. The noninteracting Green's function of electrons in d-dimensional space can be written as

$$\begin{aligned} \hat{g}^d_\sigma(\mathbf{k},\omega) &\equiv \langle\langle \Psi_{\mathbf{k}\sigma} | \Psi^\dagger_{\mathbf{k}\sigma} \rangle\rangle_\omega \big|_{U=0} \\ &= \begin{pmatrix} \omega - \varepsilon_c + \mu_\sigma & 2t\cos\frac{k_1}{2} & \cdots & 2t\cos\frac{k_d}{2} \\ 2t\cos\frac{k_1}{2} & \omega + \mu_\sigma & \cdots & 0 \\ \vdots & \vdots & \ddots & \vdots \\ 2t\cos\frac{k_d}{2} & 0 & \cdots & \omega + \mu_\sigma \end{pmatrix}^{-1}. \end{aligned} \tag{4}$$

This matrix can analytically be inverted. We obtain its determinant

$$\det\left\{\left[\hat{g}^d_\sigma(\mathbf{k},\omega)\right]^{-1}\right\} = (\omega+\mu_\sigma)^{d-1}\left[(\omega+\mu_\sigma)(\omega+\mu_\sigma-\varepsilon_c) - 4t^2\sum_{i=1}^{d}\cos^2\frac{k_i}{2}\right]. \quad (5)$$

The zeros of this determinant indicate the spectra of the Hamiltonian in Eq. (2). There are $(d-1)$ zero spectra and 2 other dispersive spectra, which satisfy the secular equation

$$\varepsilon_{\mathbf{k}\nu}(\varepsilon_{\mathbf{k}\nu}-\varepsilon_c) - 4t^2\sum_{i=1}^{d}\cos^2\frac{k_i}{2} = 0. \quad (6)$$

The dispersive spectra $\varepsilon_{\mathbf{k}\nu}$ depend on momenta through $4t^2\sum_{i=1}^{d}\cos^2\frac{k_i}{2}$. We introduce a bare density of states (DOS)

$$N_d(\epsilon) = \frac{1}{N_c}\sum_{\mathbf{k}}|\epsilon|\delta\left(\epsilon^2 - 4t^2\sum_{i=1}^{d}\cos^2\frac{k_i}{2}\right) = |\epsilon|\rho_d(\epsilon^2), \quad (7)$$

where

$$\rho_d(x) = \frac{1}{N_c}\sum_{\mathbf{k}}\delta\left(x - 2t^2 d - 2t^2\sum_{i=1}^{d}\cos k_i\right).$$

Here, we do not include the energy level ε_c in this bare DOS, because we only use this bare DOS for performing the sums over momenta in the Brillouin zone. The bare DOS can be determined by using the Fourier transform [41]

$$\Phi_d(s) = \int_{-\infty}^{\infty} dx e^{isx}\rho_d(x) = \exp\{is2t^2 d + d\ln[J_0(2t^2 s)]\}, \quad (8)$$

where $J_0(x)$ is the zeroth-order Bessel function. By expanding the exponent argument in Eq. (8) in powers of s, we obtain

$$\Phi_d(s) = \exp\left[is2t^2 d - d\frac{(2t^2 s)^2}{4} - \frac{d}{4}\left(\frac{(2t^2 s)^2}{4}\right)^2 + O(d(t^2 s)^6)\right]. \quad (9)$$

In the limit $d\to\infty$, $\Phi_d(s)$ is finite and $\rho_d(x)$ is nonvanishing if and only if t is scaled as $\sim 1/\sqrt{d}$. This scaling is identical to the one in the hypercubic and hyperdiamond lattices [36,37,42]. We take $t = t^*/\sqrt{2d}$, where t^* is a constant. Then in the infinite-dimensional limit the bare DOS becomes

$$N(\epsilon) = \lim_{d\to\infty} N_d(\epsilon) = \tfrac{1}{2}[\delta(\epsilon - t^*) + \delta(\epsilon + t^*)]. \quad (10)$$

At infinite dimensions the bare DOS has a simple form. It is just the sum of two delta functions located at $\pm t^*$. The actual bare DOS for the two dispersive bands in the infinite-dimensional limit reads

$$\tilde{N}(\epsilon) = \lim_{d\to\infty}\frac{1}{2N_c}\sum_{\mathbf{k},\nu}\delta(\epsilon - \varepsilon_{\mathbf{k}\nu}) = \tfrac{1}{2}[\delta(\epsilon-\varepsilon_+) + \delta(\epsilon-\varepsilon_-)], \quad (11)$$

where $\varepsilon_\pm = \varepsilon_c/2 \pm [\varepsilon_c^2/4 + (t^*)^2]^{1/2}$. As we have noticed the tight-binding model on the d-dimensional hyper-perovskite lattice has two dispersive bands and $(d-1)$ degenerate flat bands at zero energy. At infinite dimensions, the two dispersive bands also effectively become flat at energy level $\varepsilon_\pm$.

Inverting the matrix in Eq. (4), we obtain the noninteracting Green's functions of c and a electrons in d-dimensional space:

$$g^d_{c\sigma}(\mathbf{k},\omega) = \langle\langle c_{\mathbf{k}\sigma}|c^\dagger_{\mathbf{k}\sigma}\rangle\rangle_\omega\big|_{U=0} = \frac{\omega+\mu_\sigma}{(\omega-\varepsilon_c+\mu_\sigma)(\omega+\mu_\sigma) - 4t^2\sum_{i=1}^{d}\cos^2\frac{k_i}{2}},$$

$$g^d_{al\sigma}(\mathbf{k},\omega) = \langle\langle a_{\mathbf{k}l\sigma}|a^\dagger_{\mathbf{k}l\sigma}\rangle\rangle_\omega\big|_{U=0} = \frac{1}{\omega+\mu_\sigma}\left[1 + \frac{4t^2\cos^2\frac{k_l}{2}}{(\omega+\mu_\sigma-\varepsilon_c)(\omega+\mu_\sigma) - 4t^2\sum_{i=1}^{d}\cos^2\frac{k_i}{2}}\right],$$

$$g^d_{cal\sigma}(\mathbf{k},\omega) = \langle\langle c_{\mathbf{k}\sigma}|a^\dagger_{\mathbf{k}l\sigma}\rangle\rangle_\omega\big|_{U=0} = -\frac{2t\cos\frac{k_l}{2}}{(\omega-\varepsilon_c+\mu_\sigma)(\omega+\mu_\sigma) - 4t^2\sum_{i=1}^{d}\cos^2\frac{k_i}{2}},$$

$$g^d_{aall'\sigma}(\mathbf{k},\omega) = \langle\langle a_{\mathbf{k}l\sigma}|a^\dagger_{\mathbf{k}l'\sigma}\rangle\rangle_\omega\big|_{U=0} = \frac{1}{\omega+\mu_\sigma}\frac{4t^2\cos\frac{k_l}{2}\cos\frac{k_{l'}}{2}}{(\omega-\varepsilon_c+\mu_\sigma)(\omega+\mu_\sigma) - 4t^2\sum_{i=1}^{d}\cos^2\frac{k_i}{2}},$$

where $l,l' = 1,\ldots,d$, and $l\neq l'$. In real space within the unit cells, the noninteracting Green's functions read

$$g^d_{c\sigma}(\omega) = \langle\langle c_{I\sigma}|c^\dagger_{I\sigma}\rangle\rangle_\omega\big|_{U=0} = \frac{1}{N_c}\sum_{\mathbf{k}} g^d_{c\sigma}(\mathbf{k},\omega), \quad g^d_{al\sigma}(\omega) = \langle\langle a_{Il\sigma}|a^\dagger_{Il\sigma}\rangle\rangle_\omega\big|_{U=0} = \frac{1}{N_c}\sum_{\mathbf{k}} g^d_{al\sigma}(\mathbf{k},\omega),$$

$$g^d_{cal\sigma}(\omega) = \langle\langle c_{I\sigma}|a^\dagger_{Il\sigma}\rangle\rangle_\omega\big|_{U=0} = \frac{1}{N_c}\sum_{\mathbf{k}} g^d_{cal\sigma}(\mathbf{k},\omega)e^{-ik_l/2}, \quad g^d_{aall'\sigma}(\omega) = \langle\langle a_{Il\sigma}|a^\dagger_{Il'\sigma}\rangle\rangle_\omega\big|_{U=0} = \frac{1}{N_c}\sum_{\mathbf{k}} g^d_{aall'\sigma}(\mathbf{k},\omega)e^{i(k_l-k_{l'})/2}.$$

At large dimensions $t\sim 1/\sqrt{d}$, the diagonal Green's functions $g^d_{c\sigma}(\omega), g^d_{al\sigma}(\omega)\sim 1/d^0$, while the nondiagonal Green's functions

$$g^d_{cal\sigma}(\omega) = -\int_{-\infty}^{\infty} d\epsilon N_{d-1}(\epsilon)\int_{-\pi}^{\pi}\frac{dk_l}{2\pi}\frac{2t\cos\frac{k_l}{2}e^{-ik_l/2}}{(\omega-\varepsilon_c+\mu_\sigma)(\omega+\mu_\sigma) - \epsilon - 4t^2\cos^2\frac{k_l}{2}} \sim \frac{1}{\sqrt{d}},$$

$$g^d_{aall'\sigma}(\omega)=\frac{1}{\omega+\mu_\sigma}\int_{-\infty}^{\infty}d\epsilon N_{d-2}(\epsilon)\int_{-\pi}^{\pi}\frac{dk_l}{2\pi}\int_{-\pi}^{\pi}\frac{dk_{l'}}{2\pi}\frac{4t^2\cos\frac{k_l}{2}\cos\frac{k_{l'}}{2}e^{i(k_l-k_{l'})/2}}{(\omega-\varepsilon_c+\mu_\sigma)(\omega+\mu_\sigma)-\epsilon-4t^2\cos^2\frac{k_l}{2}-4t^2\cos^2\frac{k_{l'}}{2}}\sim\frac{1}{d}.$$

Therefore, in the limit $d\to\infty$, only the diagonal Green's functions, $g^d_{c\sigma}(\omega)$ and $g^d_{al\sigma}(\omega)$, are finite, while nondiagonal ones, $g^d_{cal\sigma}(\omega)$ and $g^d_{aall'\sigma}(\omega)$, vanish. These features greatly simplify the DMFT.

B. Dynamical mean-field theory

The DMFT is based on the infinite-dimensional limit. In this limit the self-energy is a local function of frequency. The full Green's function satisfies the Dyson equation

$$\hat{G}_\sigma(\mathbf{k},\omega)=\left\{\left[\hat{g}^d_\sigma(\mathbf{k},\omega)\right]^{-1}-\hat{\Sigma}_\sigma(\omega)\right\}^{-1},\tag{12}$$

where $\hat{\Sigma}_\sigma(\omega)$ is the self-energy. The self-energy can be expressed by the perturbation series of the noninteracting Green functions. Since in the limit $d\to\infty$, the noninteracting Green's functions $g^d_{cal\sigma}(\omega)$ and $g^d_{aall'\sigma}(\omega)$ vanish, the nondiagonal elements of the self-energy $\hat{\Sigma}_\sigma(\omega)$ must vanish too. This property is also valid in the hyperdiamond lattice, where the unit cells have two sites [42]. Therefore, the self-energy $\hat{\Sigma}_\sigma(\omega)$ is a diagonal matrix with elements $(\Sigma_{c\sigma}(\omega),\Sigma_{a\sigma}(\omega),\ldots,\Sigma_{a\sigma}(\omega))$. The matrix in Eq. (12) can analytically be inverted. We obtain the local Green's function

$$G^d_{a\sigma}(\omega)=\int\frac{d^dk}{(2\pi)^d}G^d_{a1\sigma}(\mathbf{k},\omega)=\frac{1}{\omega+\mu_\sigma-\Sigma_{a\sigma}(\omega)}+\frac{1}{\omega+\mu_\sigma-\Sigma_{a\sigma}(\omega)}\int_{-\pi}^{\pi}\frac{dk_1}{2\pi}\times\int d\epsilon N_{d-1}(\epsilon)\frac{4t^2\cos^2\frac{k_1}{2}}{[\omega+\mu_\sigma-\varepsilon_c-\Sigma_{c\sigma}(\omega)][\omega+\mu_\sigma-\Sigma_{a\sigma}(\omega)]-4t^2\cos^2\frac{k_1}{2}-\epsilon^2}.\tag{13}$$

In the limit $d\to\infty$ the last term in Eq. (13) vanishes, since $t\sim1/\sqrt{d}$, and $\lim_{d\to\infty}N_{d-1}(\epsilon)=N(\epsilon)$. Thus, the local Green's function of a electrons at infinite dimensions becomes

$$G_{a\sigma}(\omega)=\lim_{d\to\infty}G^d_{a\sigma}(\omega)=\frac{1}{\omega+\mu_\sigma-\Sigma_{a\sigma}(\omega)}.\tag{14}$$

This local Green's function has a very simple form. It looks like the full dressed Green's function of a single level μ_σ. Moreover, the local Green's function of a electrons is independent of the dynamics of c electrons. Within the DMFT the self-energy $\Sigma_{a\sigma}(\omega)$ is determined from the dynamics of a single site embedded in an effective medium. This dynamics is equivalent to the one of an Anderson model, which describes an impurity coupled with a bath [37]:

$$H^a_{d\to\infty}=-\sum_\sigma\mu_\sigma a^\dagger_\sigma a_\sigma+Un^a_\uparrow n^a_\downarrow+\sum_{m,\sigma}V^a_{m\sigma}b^\dagger_{m\sigma}a_\sigma+\text{H.c.}+\sum_{m,\sigma}E^a_{m\sigma}b^\dagger_{m\sigma}b_{m\sigma},\tag{15}$$

where $b^\dagger_{m\sigma}$, $b_{m\sigma}$ are the creation and annihilation operators that represent the bath. The bath parameters $E^a_{m\sigma}$ and $V^a_{m\sigma}$ are determined by the self-consistent equation

$$\Delta_{a\sigma}(\omega)=\sum_m\frac{|V^a_{m\sigma}|^2}{\omega-E^a_{m\sigma}},\tag{16}$$

where $\Delta_{a\sigma}(\omega)=\omega+\mu_\sigma-\Sigma_{a\sigma}(\omega)-G^{-1}_{a\sigma}(\omega)$ [37]. For most common lattices, the self-consistent equation cannot directly be solved. The bath parameters are usually determined approximately by minimizing a distance between $\Delta_{a\sigma}(\omega)$ and its projection into a finite set of the bath orbits [37]. In contrast, for the infinite-dimensional hyper-perovskite lattice, the self-consistent equation is exactly solvable. Indeed, using Eq. (14), we immediately obtain $\Delta_{a\sigma}(\omega)=0$, which leads to $V^a_{m\sigma}=0$. Therefore, the effective single-site Hamiltonian reads

$$H^a_{d\to\infty}=-\sum_\sigma\mu_\sigma a^\dagger_\sigma a_\sigma+Un^a_\uparrow n^a_\downarrow.\tag{17}$$

One can check that this effective Hamiltonian indeed yields the Dyson equation (14). It is just the single-site Hubbard model. We obtain the self-energy and the Green's function [33]

$$\Sigma_{a\sigma}(\omega)=U\langle n^a_{-\sigma}\rangle+\frac{U^2\langle n^a_{-\sigma}\rangle(1-\langle n^a_{-\sigma}\rangle)}{\omega+\mu_\sigma-U(1-\langle n^a_{-\sigma}\rangle)},\tag{18}$$

$$G_{a\sigma}(\omega)=\frac{1-\langle n^a_{-\sigma}\rangle}{\omega+\mu_\sigma}+\frac{\langle n^a_{-\sigma}\rangle}{\omega+\mu_\sigma-U},\tag{19}$$

where $\langle n^a_\sigma\rangle$ is the average occupation number of electrons at the sublattice A. It can be computed from the Green's function. From Eq. (19) we obtain

$$\langle n^a_\sigma\rangle=(1-\langle n^a_{-\sigma}\rangle)f(-\mu_\sigma)+\langle n^a_{-\sigma}\rangle f(U-\mu_\sigma),\tag{20}$$

where $f(x)=1/[\exp(x/T)+1]$ is the Fermi-Dirac distribution function at temperature T. At finite temperature ($T>0$) we always obtain $\lim_{h\to0}(\langle n^a_\uparrow\rangle-\langle n^a_\downarrow\rangle)=0$. Therefore, the sublattice A is always paramagnetic at finite temperature when the external magnetic field is absent. However, at zero temperature, a ferromagnetic solution exists. When $0<\mu<U$ and in the limit $h\to0^+$ we obtain $\langle n^a_\uparrow\rangle=1$ and $\langle n^a_\downarrow\rangle=0$. The magnetic field $h\geqslant0$ fixes the direction of magnetization. The spontaneous ferromagnetic state is fully saturated. The ferromagnetism at half filling is due to the flat feature of the electron bands of a electrons. Electrons tend to be spin polarized to minimize the Coulomb interaction energy without any cost in the kinetic energy.

Proceeding with c electrons we obtain the local Green's function

$$G^d_{c\sigma}(\omega) = \int \frac{d^d k}{(2\pi)^d} G^d_{c\sigma}(\mathbf{k},\omega),$$

where

$$G^d_{c\sigma}(\mathbf{k},\omega) = \left[\omega - \varepsilon_c + \mu_\sigma - \Sigma^d_{c\sigma}(\omega) - \frac{4t^2 \sum_{i=1}^d \cos^2 \frac{k_i}{2}}{\omega + \mu_\sigma - \Sigma^d_{a\sigma}(\omega)}\right]^{-1}.$$

In the limit of infinite dimensions we obtain

$$G_{c\sigma}(\omega) = \lim_{d\to\infty} G^d_{c\sigma}(\omega) = \frac{1}{\omega + \mu_\sigma - \varepsilon_c - \Sigma_{c\sigma}(\omega) - t^{*2} G^a_\sigma(\omega)}. \quad (21)$$

Within the DMFT the self-energy $\Sigma_{c\sigma}(\omega)$ is determined from the dynamics of a single impurity coupled with an effective conduction bath. The effective Hamiltonian reads

$$H^c_{\rm eff} = \sum_\sigma (\varepsilon_c - \mu_\sigma) c^\dagger_\sigma c_\sigma + U n^c_\uparrow n^c_\downarrow + \sum_{m,\sigma} V^c_{m\sigma} d^\dagger_{m\sigma} c_\sigma + \text{H.c.} + \sum_{m,\sigma} E^c_{m\sigma} d^\dagger_{m\sigma} d_{m\sigma}, \quad (22)$$

where $d^\dagger_{m\sigma}$, $d_{m\sigma}$ are the creation and annihilation operators that represent the bath. The bath parameters $E^c_{m\sigma}$ and $V^c_{m\sigma}$ are again determined by the self-consistent equation [37]

$$\Delta_{c\sigma}(\omega) = \sum_m \frac{|V^c_{m\sigma}|^2}{\omega - E^c_{m\sigma}} = \frac{t^{*2}\left(1 - \langle n^a_{-\sigma}\rangle\right)}{\omega + \mu_\sigma} + \frac{t^{*2}\langle n^a_{-\sigma}\rangle}{\omega + \mu_\sigma - U}. \quad (23)$$

This equation gives $V^c_{1\sigma} = t^*\sqrt{1 - \langle n^a_{-\sigma}\rangle}$, $E^c_{1\sigma} = -\mu_\sigma$ and $V^c_{2\sigma} = t^*\sqrt{\langle n^a_{-\sigma}\rangle}$, $E^c_{2\sigma} = U - \mu_\sigma$. Therefore, the effective Hamiltonian which determines the self-energy of c electrons reads

$$\begin{aligned} H^c_{d\to\infty} = {} & \textstyle\sum_\sigma (\varepsilon_c - \mu_\sigma) c^\dagger_\sigma c_\sigma + U n^c_\uparrow n^c_\downarrow \\ & + t^* \textstyle\sum_\sigma \sqrt{1 - \langle n^a_{-\sigma}\rangle} (c^\dagger_\sigma d_{1\sigma} + \text{H.c.}) \\ & - \textstyle\sum_\sigma \mu_\sigma d^\dagger_{1\sigma} d_{1\sigma} + t^* \sum_\sigma \sqrt{\langle n^a_{-\sigma}\rangle} (c^\dagger_\sigma d_{2\sigma} + \text{H.c.}) \\ & + \textstyle\sum_\sigma (U - \mu_\sigma) d^\dagger_{2\sigma} d_{2\sigma}. \end{aligned} \quad (24)$$

One can check that this effective Hamiltonian indeed yields the Dyson equation (21). It also shows a virtual hybridization between the macroscopically degenerate flat bands and the dispersive bands. In contrast to the hypercube or hyperdiamond lattices [36,37,42], the self-consistent equations of the DMFT for the infinite-dimensional hyper-perovskite lattice can analytically be solved. This allows us to explicitly construct the effective impurity Hamiltonian as in Eqs. (17) and (24). So far, the infinite-dimensional hyper-perovskite lattice is a unique lattice structure, where the self-consistent equations of the DMFT are exactly solvable. Since the DMFT is exact in the infinite-dimensional limit, this also makes the Hubbard model on the infinite-dimensional hyper-perovskite lattice exactly solvable.

At zero temperature and $0 < \mu < U$, $\langle n^a_\uparrow\rangle = 1$, $\langle n^a_\downarrow\rangle = 0$, we obtain

$$\begin{aligned} H^c_{d\to\infty} = {} & \textstyle\sum_\sigma (\varepsilon_c - \mu - \sigma h) c^\dagger_\sigma c_\sigma + U n^c_\uparrow n^c_\downarrow \\ & + t^*(c^\dagger_\uparrow d_{1\uparrow} + d^\dagger_{1\uparrow} c_\uparrow) - (\mu + h) d^\dagger_{1\uparrow} d_{1\uparrow} \\ & + t^*(c^\dagger_\downarrow d_{2\downarrow} + d^\dagger_{2\downarrow} c_\downarrow) + (U - \mu + h) d^\dagger_{2\downarrow} d_{2\downarrow}. \end{aligned} \quad (25)$$

This effective Hamiltonian just describes an impurity coupled with two bath levels with different bare energy levels. However, each spin component of the impurity is only coupled with one energy level. Therefore, the energy level splitting can lead on an imbalance of the spin population, which yields the ferromagnetism of the hypercube C. This ferromagnetism arises due to the flat-band ferromagnetism of the sublattice A, irrespective of the Coulomb interaction of c electrons. When the sublattice A is paramagnetic, this ferromagnetic mechanism is no longer valid, since both spin components of the c electron are equally coupled with the bath energy levels. In contrast to the case of the sublattice A, the effective Hamiltonian in Eq. (25) may not give a final analytical formula for the impurity Green's function. However, we can compute the impurity Green's function by exact diagonalization. In the limit $h \to 0$, we also compute the filling and the magnetization of c electrons:

$$n_c = \sum_\sigma \langle n^c_\sigma\rangle, \quad (26)$$

$$m_c = \begin{cases} \frac{1}{2}\frac{\langle n^c_\uparrow\rangle - \langle n^c_\downarrow\rangle}{n_c}, & \text{if } n_c \leqslant 1, \\ \frac{1}{2}\frac{\langle n^c_\uparrow\rangle - \langle n^c_\downarrow\rangle}{2 - n_c}, & \text{if } n_c > 1. \end{cases} \quad (27)$$

Here when $n_c > 1$ we have defined the magnetization of hole particles. When $m_c = 0$ the ground state of the hypercube C is paramagnetic. When $0 < |m_c| < 1/2$ the hypercube C is ferromagnetic and unsaturated, and when $|m_c| = 1/2$ it is also ferromagnetic, but fully saturated. If $m_c > 0$ the spin of electrons in the hypercube C is parallel to the spin of electrons in the sublattice A. In this case the full lattice is ferromagnetic. If $m_c < 0$ the magnetization of the hypercube C has the opposite direction to the one of the A sublattice. In this case the full lattice is ferrimagnetic.

We compute the self-energy $\Sigma_{c\sigma}(\omega)$ from the effective Hamiltonian in Eq. (25) by exact diagonalization at zero temperature. We are interested in the region $0 < \mu < U$, where electrons in the sublattice A form a fully saturated ferromagnetic ground state. In Fig. 2 we plot the filling of c electrons as a function of their bare energy level ε_c. Since we choose $\mu = U/2$ the system has particle-hole symmetry. In Fig. 2 one can see that the filling n_c is uniquely determined in three different regions, where n_c is around 0 (dilute electron filling), 1 (half filling), and 2 (dilute hole filling). At certain values of ε_c/t^* the filling n_c abruptly changes, and its value becomes uncertain. This signals a phase separation at those values of ε_c.

In Fig. 3 we plot the dependence of the magnetization m_c on the filling n_c for different values of the chemical potential μ. We use the energy level ε_c to vary the filling value n_c. The phase separation is the region where the filling value

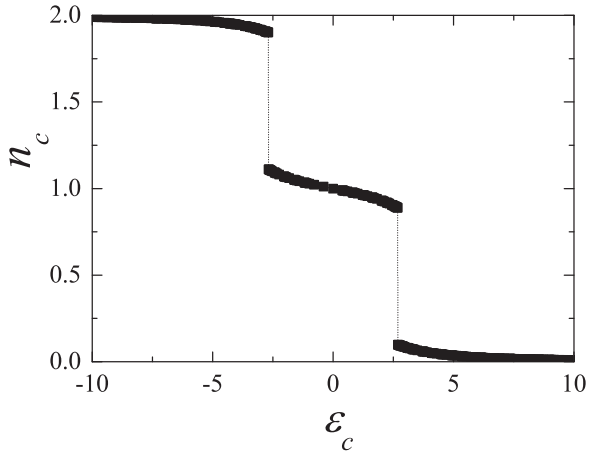

FIG. 2. The filling n_c of c electrons as a function of the energy level ε_c at $U = 5$ and $\mu = U/2$ ($t^* = 1$).

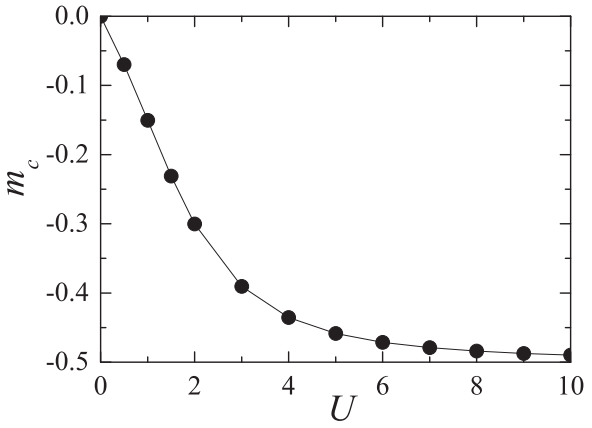

FIG. 4. The magnetization m_c of the hypercube C as a function of the Coulomb interaction U at half filling $\mu = U/2$ and $\varepsilon_c = 0$. $t^* = 1$.

n_c becomes uncertain. When $\mu \ll U/2$, the phase separation occurs around the half filling. Outside the phase separation region, for filling $n_c < 1$, $m_c = 1/2$, hence the hypercube C is fully saturated ferromagnetic, whereas in the region $1 < n_c < 2$, $-1/2 < m_c < 0$, thus the hypercube C is still ferromagnetic, but its magnetization is unsaturated. For the full lattice, when $n_c < 1$ the ground state is fully saturated ferromagnetic, while when $1 < n_c < 2$, the ground state is ferrimagnetic, since the magnetization of the hypercube m_c is negative. The phase separation separates the ferromagnetic and

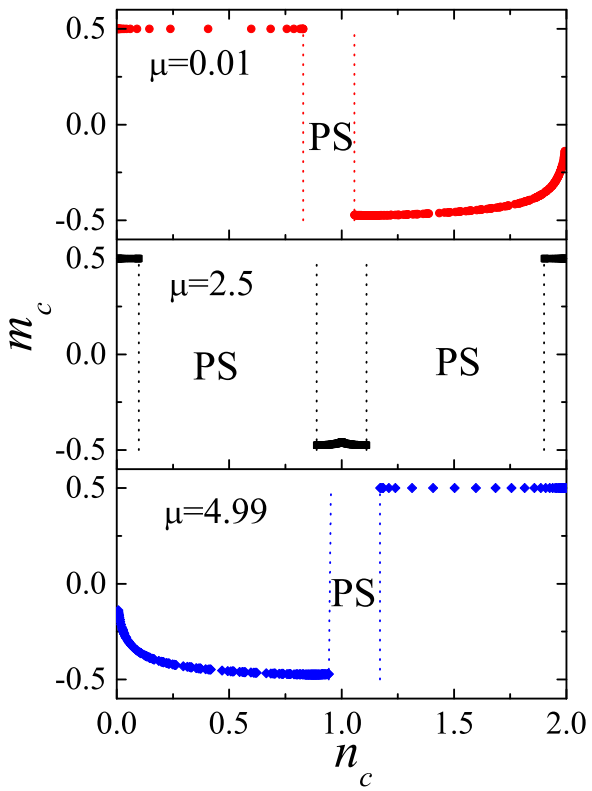

FIG. 3. The magnetization m_c via the filling n_c of c electrons for different values of the chemical potential μ. PS denotes the phase separation region. $U = 5$, $t^* = 1$.

the ferrimagnetic phases. In contrast to the two-dimensional case, where a crossover from ferromagnetism to ferrimagnetism is driven by the Coulomb interaction [15], we found the phase separation between the ferromagnetic-ferrimagnetic phase transition driven by the energy level splitting. Indeed, in the infinite-dimensional limit, all bands effectively become flat, and any finite value of the Coulomb interaction would be dominant and it cannot lead to any phase crossover. Instead of the Coulomb interaction, the energy level splitting drives the imbalance of the spin populations that lead to the ferromagnetic-ferrimagnetic phase transition through the phase separation region. With further increasing μ, the phase separation is shifted to the region of lower fillings, and an additional phase separation region appears in the filling region $n_c > 1$. When $\mu = U/2$, these two phase separation regions divide the filling n_c into three regions. At dilute electron or hole fillings, the hypercube C is fully saturated ferromagnetic, while near half filling, it is unsaturated ferromagnetic. When $\mu > U/2$, the above analyzed scenario still occurs with particles replaced by holes. Note that for all values of the chemical potential in the range $0 < \mu < U$, the filling of electrons in the sublattice A is always $n_a = 1$. The ground state is uniquely determined by the model parameters μ and ε_c rather than by ε_c and the total filling $n = n_a + n_c$. With a fixed total filling n, multiple values of the chemical potential may be obtained, and different ground states may be established.

In Fig. 4 we plot the magnetization m_c of the hypercube C as a function of the Coulomb interaction U at half filling $\mu = U/2$ and $\varepsilon_c = 0$. One can see that m_c approaches $-1/2$ only at $U \to \infty$. At finite values of the Coulomb interaction, the ferromagnetic ground state of the hypercube C is unsaturated at half filling. However, near the half filling the spin polarization of the ferromagnetism of the hypercube C is opposite to the one of the sublattice A. As a consequence, the ground state of the full lattice is ferrimagnetic. This is consistent with the Lieb theorem [35], since the sublattices C and A have unequal numbers of sites. Note in the two-dimensional Lieb lattice, the DMFT also found the ferrimagnetic ground state, however, only in the strong-coupling regime [15]. In addition, the origin of the ferrimagnetism is quite different. The ferrimagnetism found in the two-dimensional Lieb lattice is due to the

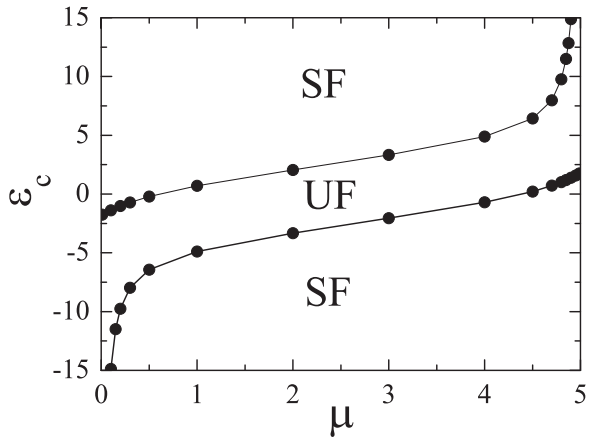

FIG. 5. Magnetic phase diagram of the hypercube C. SF (UF) denotes the fully saturated (unsaturated) ferromagnetism. The phase separation occurs on the phase boundaries. $U = 5, t^* = 1$.

antiferromagnetic Heisenberg exchange in the strong-coupling regime [15], while in the infinite-dimensional hyper-perovskite lattice the ferrimagnetism arises from the band flatness and the virtual hybridization between macroscopically degenerate flat bands and the dispersive bands.

Finally, the phase diagram is presented in Fig. 5. The phase diagram distinguishes three regions, two of which are saturated ferromagnetism ($m_c = 1/2$) separated by an unsaturated ferromagnetism region ($-1/2 < m_c < 0$). The phase boundaries are actually the phase separation, where the filling n_c becomes uncertain. For the full lattice, the saturated ferromagnetism region corresponds to fully ferromagnetism, whereas the unsaturated one corresponds to ferrimagnetism. At half filling $\mu = U/2$ and $\varepsilon_c = 0$, the ground state is ferrimagnetic.

C. Application for finite-dimensional perovskite lattices

The effective single-impurity models defined in Eqs. (17) and (24) exactly treat the local dynamics of electrons in the hyper-perovskite lattice, however, only in the infinite-dimensional limit. One can see that the effective single-impurity model of a electrons in Eq. (17) would produce the two Hubbard subbands located at $-\mu$ and $U - \mu$. In the two-dimensional case this only roughly agrees with the NRG results in the strong-coupling regime [15]. In finite-dimensional perovskite lattices the dynamical mean fields $\delta\Delta_{a\sigma}(\omega) \equiv \Delta_{a\sigma}(\omega)$ and $\delta\Delta_{c\sigma}(\omega) \equiv [\Delta_{c\sigma}(\omega) - (t^*)^2 G_{a\sigma}(\omega)]$ no longer vanish. Therefore the baths in the effective single-impurity models in Eqs. (17) and (24) do not well reproduce the dynamical mean fields. In order to take into account the finite values of $\delta\Delta_{a\sigma}(\omega)$ and $\delta\Delta_{c\sigma}(\omega)$ in the finite-dimensional lattices, we represent them by finite sets of orbits

$$\delta\Delta_{a\sigma}(\omega) = \sum_{m=1}^{n_s^a} \frac{|V_{m\sigma}^a|^2}{\omega - E_{m\sigma}^a}, \tag{28}$$

$$\delta\Delta_{c\sigma}(\omega) = \sum_{m=1}^{n_s^c} \frac{|V_{m\sigma}^c|^2}{\omega - E_{m\sigma}^c}. \tag{29}$$

This representation is similar to the one in the standard ED, except for the term $(t^*)^2 G_{a\sigma}(\omega)$ in $\delta\Delta_{c\sigma}(\omega)$, which is a feature of the exact solution at the infinite-dimensional limit. We will see later this term is crucial; without it the ED may produce artifact results. The dynamical mean fields $\delta\Delta_{a\sigma}(\omega)$ and $\delta\Delta_{c\sigma}(\omega)$ represent their derivations from the infinite-dimensional limit. The corresponding effective single-impurity models become

$$H^\alpha = H^\alpha_{d\to\infty} + \sum_{m,\sigma} V^\alpha_{m\sigma} f^\dagger_{m\sigma} \alpha_\sigma + \text{H.c.} + \sum_{m,\sigma} E^\alpha_{m\sigma} f^\dagger_{m\sigma} f_{m\sigma},$$

where α represents a or c electrons. $H^a_{d\to\infty}$ and $H^c_{d\to\infty}$ are already defined in Eqs. (17) and (24), respectively. As in the standard ED, the bath parameters $V^\alpha_{m\sigma}$ and $E^\alpha_{m\sigma}$ are determined by minimizing the distance

$$r = \frac{1}{M} \sum_{n=1}^{M} \omega_n^{-k} \left| \delta\Delta_{\alpha\sigma}(i\omega_n) - \sum_{m=1}^{n_s^a} \frac{|V^\alpha_{m\sigma}|^2}{i\omega_n - E^\alpha_{m\sigma}} \right|^2, \tag{30}$$

where $\omega_n = (2n-1)\pi T$ is the Matsubara frequency, M is a frequency cutoff, and k is a parameter which is introduced for better low-frequency fitting [43]. In particular, in our numerical calculations we take $k = 3$. We numerically solve the DMFT with the proposed modified ED as the impurity solver for the two-dimensional perovskite lattice (i.e., the Lieb lattice) at half filling ($\mu = U/2$, $\varepsilon_c = 0$). For integrations in the momentum space we take the square lattice of 128×128 points. The Matsubara frequency is discretized with fictitious temperature $T = 0.01t$. The ED is performed with the number of bath orbits $n_s^a = n_s^c = 3$. We have also checked the results with $n_s^a = n_s^c = 4$. We compute the DOS $\rho_{\alpha\sigma}(\omega) = \text{Im}G_{\alpha\sigma}(\omega - i\eta)/\pi$ with the delta function broadening $\eta = 0.01t$. In Fig. 6 we plot the obtained DOS by the DMFT with the modified ED, and compare them with the ones obtained by the DMFT with NRG [15] and by the DMFT with the standard ED [37,38]. The standard ED is performed with the number of bath orbits

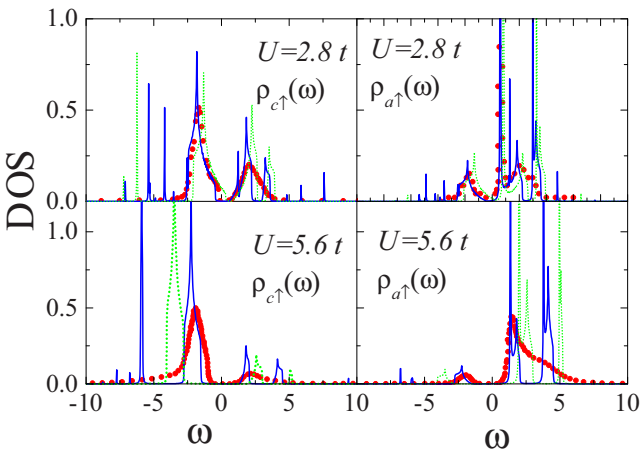

FIG. 6. The density of states (DOS) of electrons of the C and A sublattices at half filling ($\mu = U/2$, $\varepsilon_c = 0$) in the two-dimensional Lieb lattice. The blue solid lines, the green dotted lines, and the red filled circles are the DOS calculated by the DMFT with the modified ED ($n_s^c = n_s^a = 3$), the standard ED ($n_s^c = n_s^a = 5$), and the NRG, respectively. The NRG results are reproduced from Ref. [15].

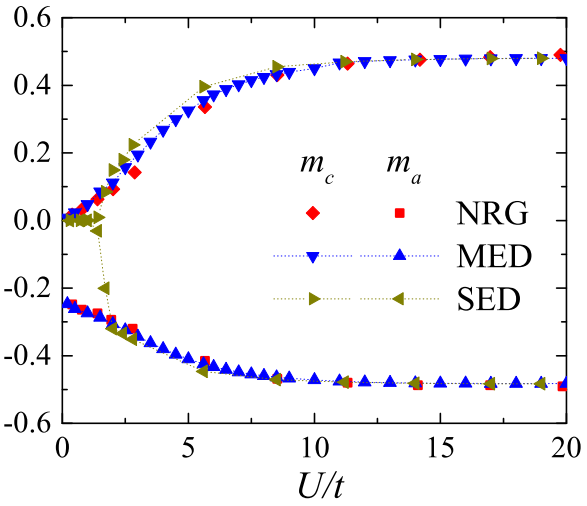

FIG. 7. The interaction dependence of the sublattice magnetizations calculated by the DMFT with NRG, the modified ED (MED) ($n_s^c = n_s^a = 3$), and the standard ED (SED) ($n_s^c = n_s^a = 5$) at half filling ($\mu = U/2$, $\varepsilon_c = 0$) in the two-dimensional Lieb lattice. The NRG results are reproduced from Ref. [15].

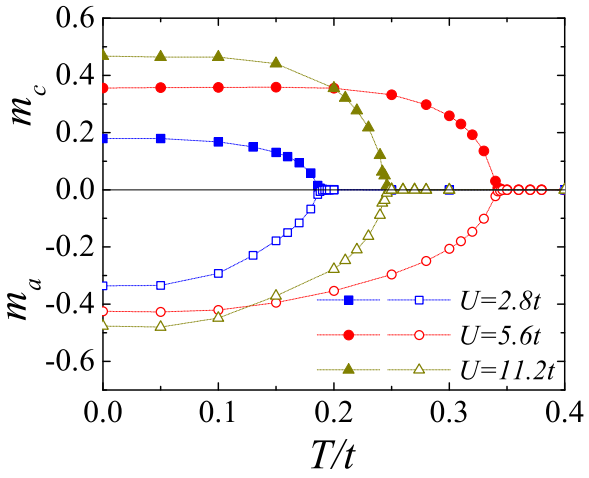

FIG. 8. The temperature dependence of the sublattice magnetizations calculated by the DMFT with the modified ED ($n_s^c = n_s^a = 3$) at half filling ($\mu = U/2$, $\varepsilon_c = 0$) in the two-dimensional Lieb lattice.

$n_s^a = n_s^c = 5$. Both the standard and modified ED have the same total number of orbits coupled to the c impurity in the ED. Like any ED, the DOSs obtained by the modified ED exhibit spikelike peaks. However, the structure of their principal peaks agrees well with the NRG results as shown in Fig. 6. In contrast, the DOSs obtained by the standard ED show significantly different behaviors. For instance, for $U = 2.8t$ the DOSs obtained by the standard ED show a metallic state, while both the NRG and the modified ED give an insulating state solution. For strong interactions ($U = 5.6t$) the principal peaks in the DOSs obtained by the standard ED are shifted from the ones obtained by the NRG and the modified ED. These results indicate that the standard procedure of minimizing the distance between the full dynamical mean field and its finite bath counterpart may produce artifacts for the flat bands. The modified ED takes into account the flat-band feature explicitly through the term $(t^*)^2 G_{a\sigma}(\omega)$. In Fig. 7 we plot the sublattice magnetizations as a function of the interaction. This figure shows good agreement between the modified ED and NRG results for whole range of the interaction, while the standard ED gives small sublattice magnetizations in the weak-interaction regime. Actually, the spontaneous magnetization of the sublattice A does not vanish as the interaction $U \to 0$ [15]. It vanishes only at $U = 0$. This feature is also confirmed by the exact solution in the infinite-dimensional limit. Due to the band flatness, any finite-value interaction would become dominant and it leads the system to the magnetically ordered state. One also can see that for weak interactions the local DOS $\rho_{a\sigma}(\omega)$ exhibits a very narrow peak due to the band flatness [15]. As a consequence, the minimizing procedure in standard ED fails to capture the flatness feature, and this induces artifacts.

As the impurity solver for the DMFT, the NRG can be extended to finite temperature [44]. However, within this NRG, it is difficult to continuously vary temperature, since temperature is discretized by a power of a cutoff [44]. In contrast, the modified ED works well with the DMFT at any temperature. It also works in both the real and imaginary frequency spaces. These features are the advantages of the ED method. In Fig. 8 we plot the temperature dependence of the sublattice magnetizations obtained by the DMFT with the modified ED. Both sublattice magnetizations vanish at the same critical temperature. This indicates that the magnetic ordering must simultaneously occur in both sublattices. Since the modified ED works well for the two-dimensional perovskite lattice, it can be used as an alternative impurity solver for three-dimensional perovskite lattice too. The modified ED can be implemented into the DFT+DMFT for electronic structure calculations [39,40]. Recently, ferromagnetism found in a number of transition-metal-oxide-based perovskites ABO_3 has attracted research attention [24–29]. In particular, the osmate-based perovskites exhibit flat-band features [29]. Most theoretical studies focus on the d electron orbitals in the transition-metal ions, and neglect their hybridizations with the p orbitals of the surrounding oxygen ions [27,28]. The hybridizations in the sharing corner octahedra BO_6 essentially yield the three-dimensional perovskite lattice. One may expect that the DFT+DMFT with the modified ED can be applied for the electronic structure calculations of those materials.

III. CONCLUSION

We have investigated the nature of the magnetically ordered phase in the Hubbard model on the infinite-dimensional hyper-perovskite lattice by using DMFT. In contrast to the hypercube or hyperdiamond lattices, for the infinite-dimensional hyper-perovskite lattice the self-consistent equations of DMFT are exactly solvable. This allows us to explicitly construct the effective impurity Hamiltonian, and makes the DMFT exact. In addition to the one-dimensional space, the hyper-perovskite lattice at infinite dimensions is the other space, where the Hubbard model is exactly solved. We have found the ferromagnetic-ferrimagnetic phase transition driven by the energy level splitting and the phase separation between the ferromagnetic and ferrimagnetic phases. Both ferromagnetism and ferrimagnetism arise from the band flatness and the virtual

hybridization between macroscopically degenerate flat bands and the dispersive bands. Our findings rigorously manifest the ferromagnetic and ferrimagnetic stabilities in a wide parameter space of the Hubbard model on the flat-band lattices. We have also proposed a modified ED as the impurity solver for DMFT on finite-dimensional perovskite lattices. The modified ED is based on the tractable analysis of the DMFT solution at the infinite-dimensional limit. It turns out that the standard ED fails to fully capture the local dynamics of the flat-band systems. As a benchmark for the modified ED, we have studied the Hubbard model on the two-dimensional Lieb lattice, and compare the obtained results with the ones calculated by DMFT+NRG. A good agreement between the modified ED and NRG results indicates a possibility of implementing the modified ED in DMFT for electronic structure calculations of flat-band materials.

ACKNOWLEDGMENTS

This research is funded by Vietnam National Foundation for Science and Technology Development (NAFOSTED) under Grant No. 103.01-2014.09.

[1] L. Zheng, L. Feng, and W. Yong-Shi, Chin. Phys. B **23**, 077308 (2014).
[2] D.-N. Sheng, Z.-C. Gu, K. Sun, and L. Sheng, Nat. Commun. **2**, 389 (2011).
[3] E. Tang, J.-W. Mei, and X.-G. Wen, Phys. Rev. Lett. **106**, 236802 (2011).
[4] K. Sun, Z. Gu, H. Katsura, and S. Das Sarma, Phys. Rev. Lett. **106**, 236803 (2011).
[5] T. Neupert, L. Santos, C. Chamon, and C. Mudry, Phys. Rev. Lett. **106**, 236804 (2011).
[6] Z. Gulácsi, A. Kampf, and D. Vollhardt, Phys. Rev. Lett. **105**, 266403 (2010).
[7] M. Maksymenko, A. Honecker, R. Moessner, J. Richter, and O. Derzhko, Phys. Rev. Lett. **109**, 096404 (2012).
[8] H. Tasaki, Prog. Theor. Phys. **99**, 489 (1998).
[9] H. Tasaki, Phys. Rev. Lett. **69**, 1608 (1992).
[10] E. C. Stoner, Rep. Prog. Phys. **11**, 43 (1946).
[11] Y. Nagaoka, Phys. Rev. **147**, 392 (1966).
[12] R. Arita, K. Kuroki, H. Aoki, A. Yajima, M. Tsukada, S. Watanabe, M. Ichimura, T. Onogi, and T. Hashizume, Phys. Rev. B **57**, R6854(R) (1998).
[13] H. Tamura, K. Shiraishi, T. Kimura, and H. Takayanagi, Phys. Rev. B **65**, 085324 (2002).
[14] S. Zhang, H.-h. Hung, and C. Wu, Phys. Rev. A **82**, 053618 (2010).
[15] K. Noda, A. Koga, N. Kawakami, and T. Pruschke, Phys. Rev. A **80**, 063622 (2009).
[16] A. Mielke, J. Phys. A **24**, L73 (1991).
[17] A. Mielke, J. Phys. A **24**, 3311 (1991).
[18] A. Mielke, J. Phys. A **25**, 4335 (1992).
[19] C. Wu, D. Bergman, L. Balents, and S. Das Sarma, Phys. Rev. Lett. **99**, 070401 (2007).
[20] C. Wu and S. Das Sarma, Phys. Rev. B **77**, 235107 (2008).
[21] S. Mukherjee, A. Spracklen, D. Choudhury, N. Goldman, P. Öhberg, E. Andersson, and R. R. Thomson, Phys. Rev. Lett. **114**, 245504 (2015).
[22] *Magnetic and Other Properties of Oxides and Related Compounds*, edited by K.-H. Hellwege and A. M. Hellwege, Landolt-Börnstein, New Series, Group III, Vol. 4, Pt. A (Springer, Berlin, 1970), p. 126.
[23] C. Weeks and M. Franz, Phys. Rev. B **82**, 085310 (2010).
[24] C.-Q. Jin, J.-S. Zhou, J. B. Goodenough, Q. Q. Liu, J. G. Zhao, L. X. Yang, Y. Yu, R. C. Yu, T. Katsura, A. Shatskiy, and E. Ito, Proc. Natl. Acad. Sci. USA **105**, 7115 (2008).
[25] J.-S. Zhou, K. Matsubayashi, Y. Uwatoko, C.-Q. Jin, J.-G. Cheng, J. B. Goodenough, Q. Q. Liu, T. Katsura, A. Shatskiy, and E. Ito, Phys. Rev. Lett. **101**, 077206 (2008).
[26] U. Lüders, W. C. Sheets, A. David, W. Prellier, and R. Frésard, Phys. Rev. B **80**, 241102(R) (2009).
[27] H. T. Dang and A. J. Millis, Phys. Rev. B **87**, 155127 (2013).
[28] Q. Han, H. T. Dang, and A. J. Millis, Phys. Rev. B **93**, 155103 (2016).
[29] M.-C. Jung and K.-W. Lee, Phys. Rev. B **90**, 045120 (2014).
[30] N. Goldman, D. F. Urban, and D. Bercioux, Phys. Rev. A **83**, 063601 (2011).
[31] M. C. Gutzwiller, Phys. Rev. Lett. **10**, 159 (1963).
[32] J. Kanamori, Prog. Theor. Phys. **30**, 275 (1963).
[33] J. Hubbard, Proc. R. Soc. London A **276**, 238 (1963).
[34] D. Vollhardt, N. Blümer, K. Held, and M. Kollar, in *Band Ferromagnetism*, edited by K. Baberschke, M. Donath, and W. Nolting, Lecture Notes in Physics Vol. 580 (Springer, Heidelberg, 2001).
[35] E. H. Lieb, Phys. Rev. Lett. **62**, 1201 (1989).
[36] W. Metzner and D. Vollhardt, Phys. Rev. Lett. **62**, 324 (1989).
[37] A. Georges, G. Kotliar, W. Krauth, and M. J. Rozenberg, Rev. Mod. Phys. **68**, 13 (1996).
[38] M. Caffarel and W. Krauth, Phys. Rev. Lett. **72**, 1545 (1994).
[39] G. Kotliar, S. Y. Savrasov, K. Haule, V. S. Oudovenko, O. Parcollet, and C. A. Marianetti, Rev. Mod. Phys. **78**, 865 (2006).
[40] K. Held, Adv. Phys. **56**, 829 (2007).
[41] E. Müller-Hartmann, Z. Phys. B **74**, 507 (1989).
[42] G. Santoro, M. Airoldi, S. Sorella, and E. Tosatti, Phys. Rev. B **47**, 16216 (1993).
[43] A. Liebsch and H. Ishida, J. Phys.: Condens. Matter **24**, 053201 (2012).
[44] R. Bulla, T. A. Costi, and D. Vollhardt, Phys. Rev. B **64**, 045103 (2001).